THE KINETICS OF CATHODIC OXYGEN REDUCTION ON THIN FILMS ON NI-CR-MO (W) ALLOYS

X. Zhang, P.Jakupi, D. Zagidulin, J.J. Noël, D. W. Shoesmith

Department of Chemistry, The University of Western Ontario, London, Ontario, N6A 5B7, Canada
E-mail: xzhan249@uwo.ca; Tel: (519) 661-2111 Ext. 86248

Abstract

The kinetics of cathodic oxygen reduction is important to the evolution of crevice corrosion of Ni-Cr-Mo (W) alloys in high temperature brines. Various electrochemical and surface analytical techniques are being employed to investigate these kinetics on oxide-covered Alloy 22 surfaces and the film properties. Potential step experiments demonstrate that steady state currents depend on temperature and applied potential. The oxygen reduction currents were significantly suppressed by the growth of a passive film. Cyclic voltammetric experiments were conducted on surfaces pre-oxidized at different potentials throughout the passive region (-0.6 V to 0.6 V vs. Ag/AgCl) and temperatures (30˚C - 90˚C) in 5 mol L^{-1} NaCl solution. The data demonstrate that the kinetics of oxygen reduction depend on both temperature and pre-oxidation potential. Oxygen reduction currents are strongly suppressed in the passive region, but revived as the potential approaches the transpassive region (> 0.4 V). With increasing temperature, the passive current increases suggesting a decrease in film resistance. TOF-SIMS depth profiles show a two-layer structure for the oxide film, with an inner region enriched in Cr_2O_3, NiO, MoO_2, WO_2, and an outer region of $Cr(OH)_3$, $Ni(OH)_2$, MoO_3, and WO_3. The thickness of the film increases with applied potential. EIS measurements show the film resistance reaches a maximum value in the passive region.

This research is supported by the Science & Technology Program of the Office of the Chief Scientist, Office of Civilian Radioactive Waste Management, U.S. Department of Energy. The work was performed under the Corrosion and Materials Performance Cooperative. DOE Cooperative Agreement Number: DE-FC28-04RW12252.

Keywords: Ni-Cr-Mo (W) Alloys, Kinetics, Oxygen reduction, Passive films

---

1. Introduction

Because of its exceptional corrosion resistance, a Ni-Cr-Mo (W) alloy, Alloy 22 (Ni-22Cr-13Mo-4Fe-3W) has been chosen as the reference material for fabrication of the outer barrier of the double-wall nuclear waste package for the Yucca Mountain repository in the U.S.A. In the development of corrosion models [1] to predict damage from the propagation of crevice corrosion, the kinetics of cathodic oxygen reduction are essential in determining passive corrosion rates, susceptibilities to localized corrosion, and propagation rates of localized corrosion processes. Despite their importance, the kinetics of this reaction have not been extensively studied on oxide-covered Ni-Cr-Mo (W) alloys.

It has been firmly established that in aqueous (neutral and alkaline) solutions, the cathodic reduction of O_2 proceeds along one, or both, of the following two pathways [2]:

(a) Direct four-electron transfer process

$$O_2 + 2H_2O + 4e^- \rightarrow 4OH^- \qquad E_{SHE}^0 = 0.401V \qquad (1)$$

(b) Two consecutive two-electron transfer processes involving the intermediate production of hydrogen peroxide

$$O_2 + 2H_2O + 2e^- \rightarrow H_2O_2 + 2OH^- \qquad E_{SHE}^0 = -0.065V \qquad (2)$$

The influence of passive films on O_2 reduction kinetics is known to be complex [3]. The kinetics of O_2 reduction have only been explored on "bare" Alloy 22 over wide ranges of pH and temperature [4]. A diffusion limiting current was found for high cathodic potentials at pH ≥ 4. The limiting current density increased over the temperature range from 20^0C to 70^0C, but decreased with a further temperature increase to 95^0C. A dual-wave polarization curve, indicating two consecutive two-electron transfer processes and the formation of the intermediate, H_2O_2, was observed only at 70 and 95^0C. Recently, it was found that increased O_2 concentrations resulted in increased corrosion potentials and corrosion rates of Alloy 625 (Ni-23Cr-10Mo-5Nb) in ammoniacal sulfate solution from 25 to 200^0C [5]. The corrosion rate became increasingly diffusion controlled as temperature and oxygen partial pressure were increased, reportedly as the barrier layer thickness and resistance decreased with temperature.

Despite these efforts, the influence of the oxide film on Alloy 22, and similar Ni-Cr-Mo (W) alloys, on O_2 reduction is poorly characterized. Various electrochemical techniques are being employed to investigate the kinetics of O_2 reduction on Alloy 22, at temperatures up to 90^0C in saline solutions similar to those anticipated within the Yucca Mountain repository site. Surface analysis techniques, are being employed to characterize the passive film and to determine the key film properties controlling O_2 reduction kinetics.

2. Experimental

2.1. Electrochemical Experimental Setup

A standard three-electrode, glass electrochemical cell was used for all experiments. The cell contains a working electrode, a pure platinum (99.95% purity) counter electrode and an in-house fabricated silver/silver chloride (Ag/AgCl) reference electrode in saturated KCl solution (199mV vs. SHE at 25^0C). The cell has an outer jacket through which water is circulated from a thermostatic bath to maintain the temperature of the solution to within 1^oC.

5M NaCl solutions were used in all experiments. Prior to starting each experiment, the electrolyte solution was sparged for at least one hour in either Grade 4.4 oxygen or UHP argon (Praxair), and sparging was continued throughout the experiment. The solutions were maintained at pH 7.0 ± 0.2.

Electrodes were cylindrical specimens with a diameter of 1 cm and a height of 0.5-1 cm cut from plate materials. Each specimen was encased in a heat-resistant epoxy resin, and connected to a rotating disc assembly. A rotation rate of 23.3 Hz was used in experiments. Before each experiment, the working electrode (WE) was polished using 320, 600, 800, 1000 and 1200 grade silicon carbide paper in sequence, and then ultrasonically cleaned for ten minutes in methanol and finally in deionized water.

2.2. Electrochemical Experiments

Figure 1 is a schematic of the potential profile used in potential step experiments to determine the polarization curves in both O_2-sparged and Ar-sparged solutions. Figure 2 shows the potential profile used in potentiostatic and cyclic voltammetry (CV) experiments.

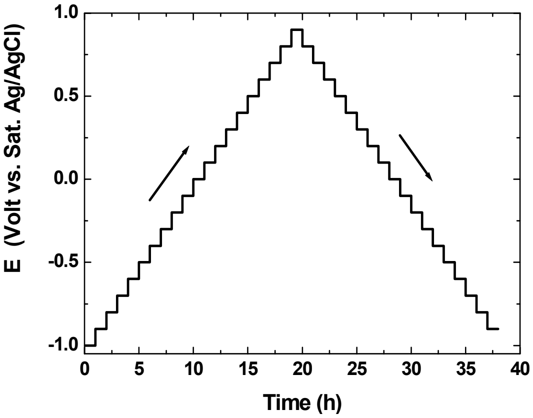

Figure 1. Schematic of potential profile used in potential step experiments

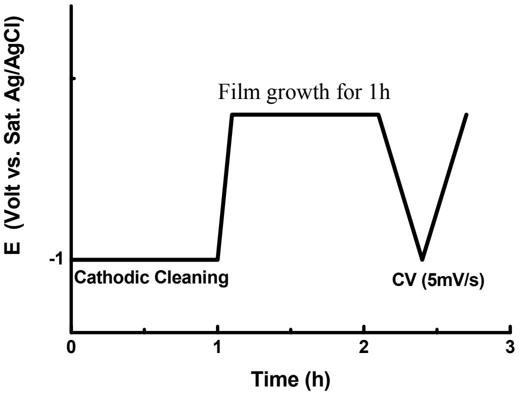

Figure 2. Schematic of potential profile used in potentiostatic and CV experiments

2.3. Surface Analysis

An ION-TOF time of flight secondary ion mass spectrometer (TOF SIMS IV) was used to obtain the depth profiles of passive films grown potentiostatically on a cathodically cleaned Alloy 22 specimen. Electrochemical impedance spectroscopic (EIS) measurements were carried out with a Solartron1287/1255B system controlled by CORRWARE and ZPLOT Software programs.

3. Results and Discussion

3.1. Polarization curves

Figure 3 compares the polarization curves recorded for Alloy 22 in O_2-sparged and Ar-sparged solutions at various temperatures. Three distinct potential regions, but no active region, were observed: a cathodic reduction region, a passive region, and a transpassive region. The passive region was wider under O_2 free conditions (-0.6V to 0.4V) than when O_2 was present (-0.3V to 0.4V), indicating that O_2 reduction was not completely suppressed by the defective oxide film until potentials > -0.3V were reached. Comparison of the cathodic reduction currents in these solutions, shows that oxygen reduction accounts for the high cathodic current density on the forward scan in O_2-sparged solution, whereas H_2O reduction occurs when $E < -0.7V$. H_2O reduction currents show a consistent temperature dependence, whereas the temperature dependence of O_2 reduction currents is complex. This is most probably caused by the competition between an increase in the mass transfer rate with increasing temperature and a considerable decrease in oxygen concentration in the bulk solution at high temperatures, as observed by Macdonald et al [4].

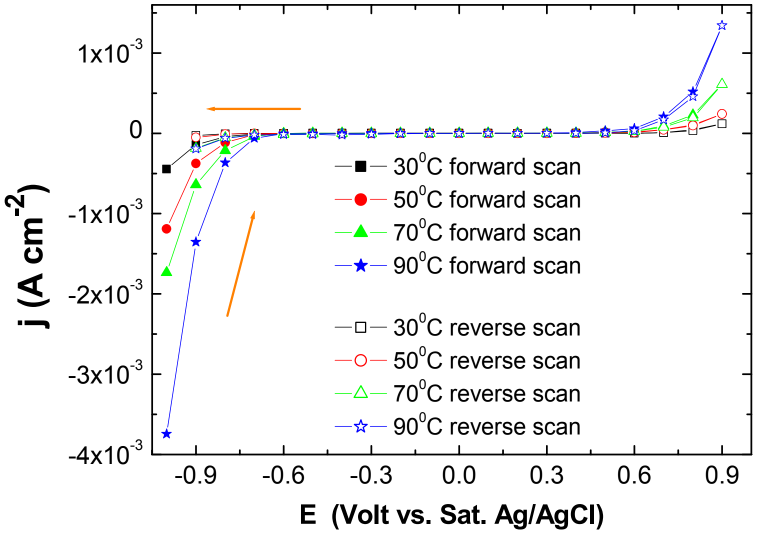

(a)

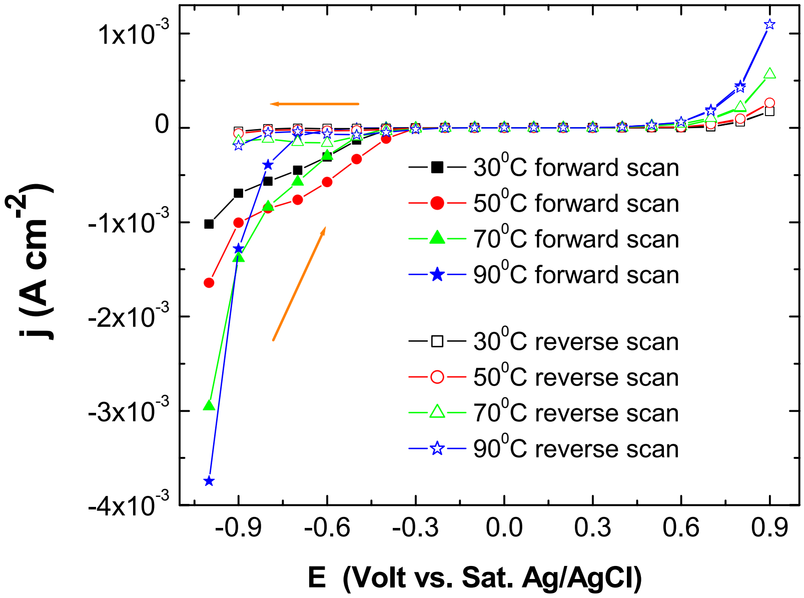

(b)

Figure 3. Polarization curves for Alloy 22 in 5M NaCl solution at 30^0C, 50^0C, 70^0C, and 90^0C: (a) in Ar-sparged solutions; (b) in O_2-sparged solutions.

The reverse scans show that the cathodic current densities for both O_2 and H_2O reduction were significantly suppressed when compared to the forward scan. This suppression is attributed to the formation of the passive oxide at positive potentials. Behavior in the passive and transpassive regions was insensitive to the presence of O_2.

3.2. Potentiostatic and Cyclic Voltammetry (CV) Experiments

Figure 4 shows current transients measured at 0 V at various temperatures in Ar-sparged solutions. It clearly shows that, at an applied potential of 0 V, the current was anodic and decreased substantially with time, indicating that passive film growth lead to the complete suppression of O_2 reduction. The passive current increases with temperature, suggesting a decrease in film resistance at high temperatures. The current transients in O_2-sparged solutions showed the similar behaviour.

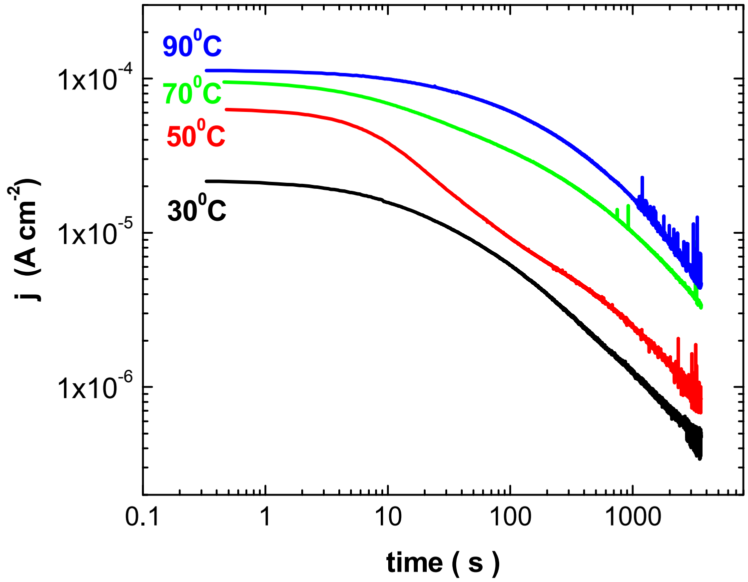

Figure 4. Current-time behaviour for oxide film growth at 0 V at various temperatures in Ar-sparged solutions.

After oxide film growth at constant potentials, the electrode potential was scanned from the holding potential to the cathodic limit of -1 V (forward scan) and back (reverse scan) (Figure 2) to measure the current for O_2 reduction on the oxide film. Figure 5 shows a series of CVs performed at 70^{0}C. The currents are shown offset to illustrate the differences. When the electrode was oxidized at low potentials ($E \leq 0$ V), reversible current-potential behaviour was observed and no O_2 reduction wave. This suggests the oxide film grown even at low potentials effectively eliminated or suppressed the O_2 reduction current on the forward scan. After oxidation at high potentials (0.4 V and 0.6 V), O_2 reduction was revived on the forward scan and a well-defined O_2 reduction wave was observed in O_2-sparged solutions, or a large film reoxidation peak on the reverse scan in Ar-sparged solutions. The size of the reoxidation peak observed in the absence of O_2 increases with the preoxidation potential, indicating the formation of a thicker, more oxidized (i.e., containing metal cations in higher oxidation states) and, hence, more defective oxide film. In O_2-sparged solutions, this leads to a revival of the O_2 reduction current.

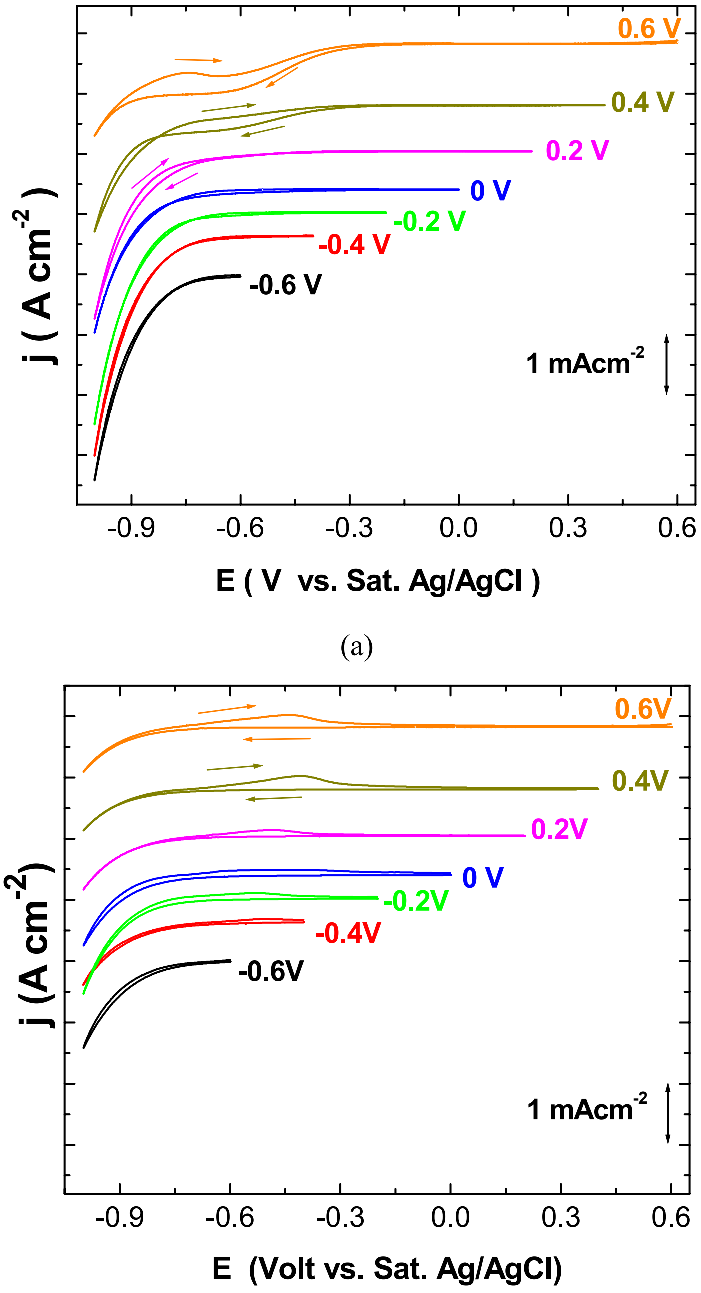

(a)

(b)

Figure 5. CVs recorded after film growth at various potentials at 70^{0}C in (a) O_2-sparged solutions; (b) Ar-sparged solutions.

3.3. Surface Analyses

Figure 6 shows TOF-SIMS depth profiles for the passive film on Alloy 22 grown at 0 V and 30^{0}C in Ar-sparged solutions. While these profiles are not quantitative, the relative distributions of the various elements and their compounds can be determined. The profiles for Ni, Cr, Mo and W, clearly show the presence of a two-layer structure for the oxide film, with an inner region enriched in Cr_2O_3, NiO, MoO_2, WO_2, and an outer region of $Cr(OH)_3$, $Ni(OH)_2$, MoO_3, and WO_3. By comparison, after oxidation at 0.6 V, the TOF-SIMS profiles show more Mo and W oxide present in the film, especially in higher oxidation states. Also, the Cr $(OH)_3$ and $Ni(OH)_2$ content of the film increases. Both effects lead to a thickening of the oxide layer.

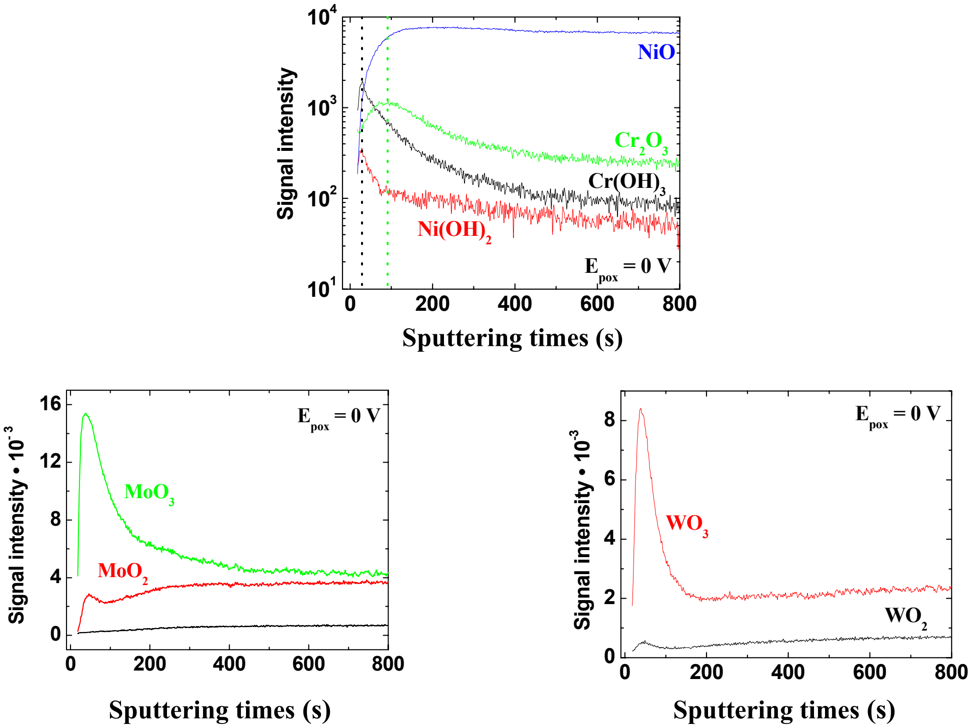

Figure 6. TOF-SIMS depth profiles for Alloy 22 after oxidation at 0 V and 30^0C in Ar-sparged solution.

The overall film resistances (from EIS measurements) as a function of film-growth potential and temperature are shown in Figure 7. The resistance shows three regions similar to those observed in electrochemical experiments and by other researchers on Ni-Cr alloys [6]. The maximum resistance of the film is observed in the range -0.4 V< E < 0.3 V; i.e., in the potential region where passive behaviour is observed. At lower potentials, the resistance increases with increasing potential, consist with defect annealing in the oxide. At potentials above 0.2 V, the resistance decreases with increasing potential, which indicates the onset of transpassive dissolution with higher oxidation states of film cations (Cr $^{3+}$ → CrO_4^{2-}, M_O $^{3+}$ → M_O $^{6+}$, and W $^{3+}$ →W $^{6+}$). These results are consistent with the electrochemical behaviour. However, the dependence of film resistance on temperature is not consistent with the electrochemical experiments, and is under further investigation.

4. Summary and Conclusions

(1) Various electrochemical and surface analytical techniques are being employed to investigate the film properties and the kinetics of O_2 reduction on oxide-covered Alloy 22 surfaces.

(2) Potential step experiments demonstrate that steady state currents depend on temperature and

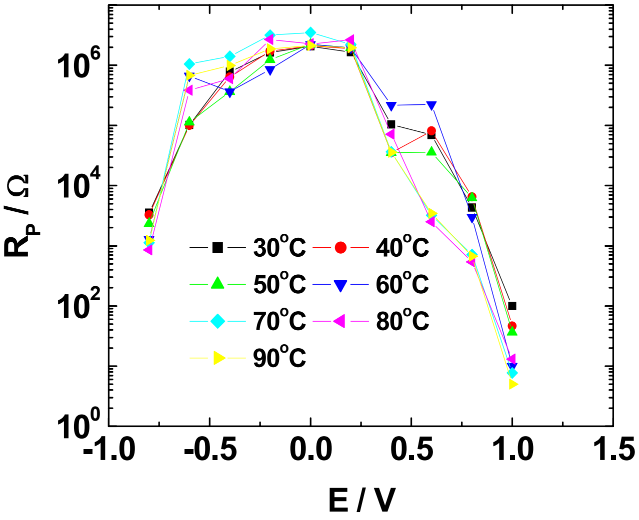

Figure 7. Film resistances as a function of film-growth potential and temperature in Ar-sparged solutions

applied potential. Three distinct regions were observed in the polarization curve for Alloy 22. The cathodic currents for both O_2 reduction and H_2O reduction were significantly suppressed by the growth of a passive film. O_2 reduction only occurs when the film is defective. While H_2O reduction currents show a consistent temperature dependence, the dependence of O_2 reduction currents on temperature is complicated.

(3) Cyclic voltammetric experiments were conducted on surfaces pre-oxidized at different potentials. The data demonstrate that the kinetics of oxygen reduction depend on both temperature and pre-oxidation potential. Oxygen reduction currents are strongly suppressed in the passive region, but revived as the potential approaches the transpassive region (E > 0.4 V).

(4) TOF-SIMS depth profiles show a two-layer structure for the oxide film, with an inner region enriched in Cr_2O_3, NiO, MoO_2, WO_2, and an outer region of $Cr(OH)_3$, $Ni(OH)_2$, MoO_3, and WO_3. The thickness of the film increases with applied potential. EIS measurements show the film resistance reaches a maximum value in the passive region, consistent with the small passive currents observed in this region in electrochemical experiments. The resistance decreases in the transpassive region, in agreement with the film transformation to more soluble states containing higher oxidation states and hydroxides.

Acknowledgements

Haynes International, Kokomo, Indiana, for their generous provision of Alloy 22 material.
Dr. James Francis in Surface Science Western for his conducting TOF-SIMS analysis.

References

[1] Alexei Davydov, Konstantin V.Rybalka, Louiza A.Beketaeva, George R.Engelhardt, Palitha Jayaweera, Digby D.Macdonald, Corrosion Sci., 47 (2005), p195

[2] V.S.Bagotskii, M.R.Tarasevich and V.Yu.Filinovskii, Calculation of the Kinetic Parameters of Coupled Reactions of Oxygen and Hydrogen Peroxide. Elektrokhimiya, 5, 1969, 1218-1221.

[3] N.Le Bozec, C.Compere, M.L'Her, A.Laouenan, D.Costa, P.Marcus, Corrosion Sci., 43 (2001), p765

[4] Alexei Davydov, Konstantin V.Rybalka, Louiza A.Beketaeva, George R.Engelhardt, Palitha Jayaweera, Digby D.Macdonald, Corrosion Sci., 47 (2005), p195

[5] Edouard Asselin, Akram Alfantazi, and Steven Rogak, Journal of The Electrochemical Society, 154 (4) (2007), p215

[6] M.Bojinov, G.Fabricius, P.Kinnunen, T.Laitinen, K.Makela, T.Saario, G.Sundholm, J.Electroanalytical Chemistry, 504 (2001), p.29